The Cryosphere Discuss., 7, 4633–4680, 2013
www.the-cryosphere-discuss.net/7/4633/2013/
doi:10.5194/tcd-7-4633-2013

The Cryosphere Discussions
Open Access

Influence of snow depth distribution on surface roughness in alpine terrain: a multi-scale approach

J. Veitinger[1], B. Sovilla[1], and R. S. Purves[2]

[1]WSL Institute for Snow and Avalanche Research SLF, Davos, Switzerland
[2]Department of Geography, University of Zurich, Zurich, Switzerland

Received: 16 July 2013 – Accepted: 12 August 2013 – Published: 13 September 2013

Correspondence to: J. Veitinger (veitinger@slf.ch)

Published by Copernicus Publications on behalf of the European Geosciences Union.

Abstract

In alpine terrain, the snow covered winter surface deviates from its underlying summer terrain due to the progressive smoothing caused by snow accumulation. Terrain smoothing is believed to be an important factor in avalanche formation, avalanche dynamics and affects surface heat transfer, energy balance as well as snow depth distribution. To characterize the effect of snow on terrain we use the concept of roughness. Roughness is calculated for several snow surfaces and its corresponding underlying terrain for three alpine basins in the Swiss Alps characterized by low medium and high terrain roughness. To this end, elevation models of winter and summer terrain are derived from high-resolution (1 m) measurements performed by airborne and terrestrial LIDAR. We showed that on basin scale terrain smoothing not only depends on mean snow depth in the basin but also on its variability. Terrain smoothing can be modelled in function of mean snow depth and its standard deviation using a power law. However, a relationship between terrain smoothing and snow depth does not exist on a pixel scale. Further we demonstrated the high persistence of snow surface roughness even in between winter seasons. Those persistent patterns might be very useful to improve the representation of a winter terrain without modelling of the snow cover distribution. This can potentially improve avalanche release area definition and in the long term natural hazard management strategies.

1 Introduction

During and after a snowfall, wind, snow gliding and avalanches redistribute snow and smooth the geomorphology of the terrain by filling irregularities and settling. During the snow accumulation season, terrain features successively disappear leading to increasingly homogeneous deposition patterns during storm events and, thus, to a progressive smoothing of the terrain surface. Terrain smoothing is believed to be an important factor in avalanche formation and dynamics. Moreover, smoothing of terrain irregularities

TCD
7, 4633–4680, 2013

by snow also affects surface heat transfer and energy balance (e.g Fassnacht et al., 2009) as well as snow depth distribution (Mott et al., 2010). Thus, understanding snow smoothing on topography is very important in avalanche hazard assessment, run-off modelling and water resource management. Further, the influence of snow surface roughness on albedo has been highlighted (e.g. Manninen et al., 2012).

The evaluation of snow's influence on topography is an important task in avalanche risk assessment and hazard mapping. To correctly estimate the run-out distance of an avalanche, a precise estimation of the avalanche release area (as well as fracture depth) and the characteristics of the avalanche track (friction, etc.) are required. Both are influenced by terrain smoothing. Terrain smoothing in an avalanche path is able to change the terrain-avalanche friction and thus has an impact on its dynamics, and is especially important in determining the location and size of avalanche release areas. The evaluation of release area size is very complex and still typically requires considerable expert knowledge and experience. Existing tools for the automatic detection of avalanche release areas (e.g. Maggioni and Gruber, 2003; Bühler et al., 2013) are exclusively based on topographical parameters and are therefore mainly suited for the definition of extreme avalanches whose extents are strongly controlled by topography. These algorithms often fail to estimate smaller avalanche release areas that vary in location and size within the same topographical basin as they neglect the effect of variations in snow cover distribution. Changing deposition patterns due to terrain smoothing could thus explain the observed differences in release areas.

The importance of snow cover distribution in avalanche formation processes is well known and mentioned in literature. One parameter particularly highlighted in this context is roughness. For a shallow snowpack, roughness can have a stabilizing function hindering the formation of continuous weak layers (Schweizer et al., 2003) and slabs (Simenhois and Birkeland, 2008) as well as providing mechanical support to the snowpack. McClung (2001) showed in a study of 76 avalanche paths due to clear- cut logging in the Coast and Columbia mountains of British Columbia, that ground roughness (defined in a categorical way: (1) low: ground features smaller than 1 m relief; (2)

TCD
7, 4633–4680, 2013

medium: ground features 1–2 m relief; (3) high: ground features bigger than 2 m relief) is potentially important in inhibiting the snowpack in the downward motion. Actually, no events were reported in areas with roughness height larger than 2 m. In a recent study, van Herwijnen and Heierli (2009) stated, that in case of weak layer failure, roughness of the bed surface plays an important role in determining if an avalanche releases or not. However these stabilizing effects of terrain roughness disappear if the snowpack is deep enough to form a relatively smooth intermediate sliding surface (McClung and Schaerer, 2002) where the formation of a homogenous snowpack with continuous weak layers and slabs is facilitated. All these studies demonstrate the ability of roughness to capture terrain smoothing as well as its importance in avalanche formation processes.

In recent years, airborne (Vallet, 2011; Fischer et al., 2011) and terrestrial laser scanning (Grünewald et al., 2010; Prokop, 2008; Prokop et al., 2008) have become increasingly reliable and feasible techniques to obtain continuous snow depth measurements even in steep alpine terrain, allowing analysis of snow depth distribution over multiple scales (Schirmer and Lehning, 2011; Deems et al., 2008; Trujillo et al., 2007). The importance of scale in snow redistribution is widely recognized. For instance it is known, that snow redistribution patterns vary over scales due to different underlying processes (Blöschl, 1999). Winstral et al. (2002) suggested that one reason for the low percentage of snow depth variation that can be explained by terrain parameters might be due to differences in modelled processes and scales. Accordingly, methods like fractal analysis were applied to evaluate snow depth variability over a wide range of scales (Schirmer and Lehning, 2011; Deems et al., 2008, 2006). Snow depth generally showed two distinct regions of fractal scaling separated by a scale break where the dynamics of the underlying processes shaping the snow cover are supposed to change. Interestingly, theses studies revealed very high interannual consistency of the fractal scaling behaviour of snow depth suggesting that observed scaling properties are characteristic of the specific site and are relatively insensitive to variations in snow accumulation (Deems et al., 2008). This result was further strengthened by Schirmer et al. (2011)

TCD
7, 4633–4680, 2013

Influence of snow depth distribution on surface roughness in alpine terrain

J. Veitinger et al.

who found very high interannual consistency of snow depth measurements. Using a fractal roughness parameter, Lehning et al. (2011) could further show that rougher terrain holds less snow than smoother terrain. Although these studies brought a lot of valuable insight into snow depth distribution and its persistent topographical control in alpine terrain, only little focus was put on how snow depth affects roughness of a winter terrain surface. Schirmer and Lehning (2011) interpreted the two distinct fractal scaling behaviours of snow depth in combination with increasing scale breaks in the accumulation season as smoothing of terrain roughness at increasing scales. Schweizer et al. (2003) stated that a snow depth of 0.3 m to 1 m is required to eliminate terrain roughness. However, a thorough analysis of the scale dependent influence of snow depth on the geomorphology of a terrain surface as well as assessing the temporal consistency of snow surface roughness has not been attempted yet.

In this study we therefore aim to characterize and quantify the smoothing effects of snow on terrain. To this end, we derive local roughness estimates of winter and summer terrain from high-resolution measurements performed by airborne and terrestrial LIDAR for three alpine basins in the Swiss Alps (Fig. 1) using a local roughness parameter derived from geomorphological parameters. Having done so, we firstly capture and quantify terrain smoothing. Secondly, we discuss the role of different terrain characteristics of three distinct basins in terrain smoothing processes. Thirdly, we link terrain smoothing to snow cover parameters. In the last part we assess the spatial interaction of snow depth and surface roughness and quantify persistence of snow depth and surface roughness patterns.

2 Surface roughness

In general we understand under roughness the variability of a topographical surface at a given scale. A number of definitions of roughness exist, for a recent overview see Grohmann et al. (2011). We decided to choose the vector ruggedness measure developed by Sappington et al. (2007) and based on the vector approach proposed by

Hobson (1972). In a first step the elevation gradient in both the x and y directions of a grid cell and its eight neighboring cells is used to calculate the magnitude (slope), α, and the direction (aspect), β, of steepest gradient (Horn, 1981). We define a, b and c as the upper left, upper central and uper right pixel respectively, d and f as the central left and central right pixel respectively and g, h and i as the lower left, lower central and lower right pixel respectively. We denote:

$$\frac{\mathrm{d}z}{\mathrm{d}x} = \frac{(c+2f+i)-(a+2d+g)}{(8\cdot \mathrm{cellsize}_x)}, \tag{1}$$

$$\frac{\mathrm{d}z}{\mathrm{d}y} = \frac{(g+2h+i)-(a+2b+c)}{(8\cdot \mathrm{cellsize}_y)}, \tag{2}$$

where $\mathrm{cellsize}_x$ and $\mathrm{cellsize}_y$ correspond to the size of the grid cell in x and y direction, respectively. Slope and aspect are then calculted using the following formulas:

$$\alpha = \arctan\left(\sqrt{\left(\frac{\mathrm{d}z}{\mathrm{d}x}\right)^2 + \left(\frac{\mathrm{d}z}{\mathrm{d}y}\right)^2}\right), \tag{3}$$

$$\beta = \arctan\left(\frac{\frac{\mathrm{d}z}{\mathrm{d}y}}{\frac{\mathrm{d}z}{\mathrm{d}x}}\right). \tag{4}$$

Based on these definitions, normal unit vectors of every grid cell of a digital elevation model (DEM) within a selected neighbourhood window are decomposed into x, y and z components (Fig. 2, Eqs. (5)–(8)):

$$z = 1 \times \cos(\alpha), \tag{5}$$

TCD
7, 4633–4680, 2013
Influence of snow depth distribution on surface roughness in alpine terrain
J. Veitinger et al.

$$xy = 1 \times \sin(\alpha), \tag{6}$$

$$x = xy \times \sin(\beta), \tag{7}$$

$$y = xy \times \cos(\beta). \tag{8}$$

The resultant vector $|r|$ is then obtained by:

$$|r| = \sqrt{(\sum x)^2 + (\sum y)^2 + (\sum z)^2}, \tag{9}$$

as shown in Fig. 2b. The magnitude of the resultant vector is then normalized by the number of grid cells n and subtracted from 1:

$$\mathrm{VRM} = 1 - \frac{|r|}{n}, \tag{10}$$

where VRM is the vector ruggedness measure.

The result is a measure of the surface roughness and values range from 0 (flat) to 1 (extremely rough). This definition allows to derive roughness directly from a DEM and the moving window technique allows us to calculate local, pixel based, estimates of roughness. By setting the neighbourhood window size, we can further account for scale. Since the method incorporates both the aspect and slope of the elevation gradient, we can distinguish between constant slope with constant aspect and constant slope with changing aspect (Fig. 2c). Sappington et al. (2007) showed that the vector ruggedness measure is uncorrelated with slope. The measure has already been applied in different research fields including among others: animal habitat analysis (Sappington et al., 2007), avalanche dynamics (Sovilla et al., 2012) and avalanche formation (Vontobel, 2011).

TCD
7, 4633–4680, 2013

3 Field sites

We focus our study on two mountain test sites located in the Swiss Alps (Fig. 3). The Steintälli site (ST) is situated in the eastern part of Switzerland near Davos. The area of the basin is 73 500 m^2. The terrain is characterized by elevations between 2418 m a.s.l. and 2600 m a.s.l. and the orientation ranges from NE through E to SE. Steep slopes are located near the ridge, flattening out in the lower part of the basin. The mean slope of the basin is 35.6° with a standard deviation of 7.3°.

The site of Vallée de la Sionne (VdlS) is located in the south-western part of Switzerland in the canton of Valais, near Sion. The terrain is characterized by elevations between 2460 m a.s.l. and 2679 m a.s.l. and the orientation ranges from E to SE. The VdlS field site is divided into two different basins characterized by distinct topography: Crêta Besse 1 (CB1) is steeper and rougher whereas Crêta Besse 2 (CB2) is less steep and shows a very homogenous terrain surface without major ridges or cliffs. The area of the basin CB1 is 52 600 m^2, its mean slope is 42.4° with a standard deviation of 6.0°. The area of the basin CB2 is 60 700 m^2 and it has a mean slope of 36.2° with a standard deviation of 3.9°.

The three basins are further characterized by different roughness distributions. Average roughness is highest for CB1 and lowest for CB2. The distribution of roughness is strongly skewed to the high values. Furthermore, average roughness increases with larger scales, whereas maximum roughness decreases.

4 Data

4.1 Steintälli

The snow distribution in the Steintälli basin was determined using terrestrial laser scanning (TLS). We performed in total 7 scans of the winter terrain between January and March within the winter seasons of 2010/11 and 2011/12. An additional scan of the summer terrain was acquired on 18 September 2011 and serves as reference for the snow depth calculations. Raster maps with a spatial resolution of 1 m were produced. To calculate snow depth HS, the summer terrain was subtracted from the winter terrain and negative snow depth values were excluded. The precision of a single scan was determined by comparing the differences of two consecutive scans of the same snow surface. Only scans with a mean precision better than 0.1 m were considered. Table 1 shows mean snow depth, $\overline{\mathrm{HS}}$, and its standard deviation, $\sigma(\mathrm{HS})$, as well as the coefficient of variation, C_v, of all snow depth acquisitions. The coefficient of variation, C_v, is a normalised measure of the variability of the snowpack defined by the standard deviation divided by the mean snow depth:

$$C_\mathrm{v} = \frac{\sigma(\mathrm{HS})}{\overline{\mathrm{HS}}}. \tag{11}$$

Snow depths in 2011/2012 were lower (1.33 m and 1.43 m respectively) than in 2011/2012 where snow depth varied between 1.91 m and 2.75 m. The coefficient of variation ranges from 0.2 to 0.37 with generally increasing values towards the end of the accumulation period. It is thus a good indicator for the increasing redistribution of the snow cover during the accumulation season. Figure 4 shows the evolution of the snow depth HS for the two winter seasons of 2010/2011 and 2011/2012 at the weather station WAN7 in close vicintity to the basin. Interestingly, the maximum snow depth was reached very early in the winter season 2011/2012, in January, and it is basically the result of one long period of intermittent snowfalls. Normally peak accumulation in these altitudes is reached later in the season (March or April). Another particular feature of the winter season 2011/12 was the presence of large glide snow cracks within the snow surface.

4.2 Vallée de la Sionne

At the Vallée de la Sionne airborne laser scanning (ALS) measurements are performed before and after avalanche events using a helicopter based system and a detailed description of the method and the precision of the measurements can be found in Sovilla et al. (2010). The accuracy of the data is 0.10 m. We resampled the original grid from 0.5 m resolution to 1 m resolution using cubic interpolation to have the same spatial resolution as in Steintälli. At the Vallée de la Sionne test site, three ALS measurements were performed in three different winter seasons. The three scans were taken at significantly different stages of the accumulation season. Figure 4 shows the evolution of snow depth HS for the winters 2005/06, 2008/09 and 2011/12 at the weather station Donin du Jour which is situated several hundred meters away from the basins. Table 2 shows the snow cover characteristics of all acquisitions for the basins CB1 and CB2. The scan acquired on the 8 March 2006 can be considered close to the peak accumulation of the winter. The scan of the 25 January 2009 is the result of several snowfalls within the winter season. Both scans show a significantly larger standard deviation. Finally, the scan of the 8 December 2011 was performed after the first significant snowfall of the winter season, and represents a very homogeneous snowpack where little redistribution has taken place.

5 Terrain smoothing on basin scale

5.1 Terrain smoothing assessment

Snow changes the underlying terrain by filling gullies and covering rocks, but also creates drift features such as dunes and cornices, which may be uncorrelated with the underlying terrain. Thus, to evaluate terrain smoothing it is necessary to both calculate the degree of attenuation of terrain features produced by snow and estimate the degree of similarity between winter and summer surface.

To quantify smoothing, we calculated roughness of the winter surface, R_S, and the corresponding summer terrain, R_T, for each 1 m grid cell within every basin. By varying the size of the moving window from 3 m up to 25 m we aimed to account for different scales. Scale in our context thus corresponds to the size of the moving window.

Figure 5 shows an example of correlation between terrain roughness, R_T, and snow surface roughness, R_S, for the CB1 basin and for a scale of 5 m and 25 m. In a first approximation, we identified in all basins a linear relationship between R_S and R_T, of the form:

$$R_S = b \times R_T, \quad (12)$$

where b is the slope of the regression fit. The slope of the regression fit is then subtracted by 1 and considered the magnitude of terrain smoothing. We denote the smoothing factor F:

$$F = 1 - b. \quad (13)$$

F ranges between 0 when surface roughness is equal to terrain roughness and no smoothing is observed, and 1 for a complete even snow surface. Theoretically, F can be negative for snow surfaces which are rougher than the terrain surface.

Further, we calculate the coefficient of determination, R^2, of the regression fit, which determines the degree of similarity between the snow surface and terrain surface. High values, up to 1, indicate that the underlying terrain is still dominating and the influence of snow is low. Low values indicate that snow influence is dominant creating significant changes of the surface structure. Both measures, F and R^2 together define terrain smoothing.

Figure 6 shows F and the coefficient of determination, R^2, of terrain roughness and snow surface roughness as a function of different scales for the basins ST, CB1 and CB2. All basins show a decreasing smoothing factor F with increasing scales. The correlation between terrain and surface roughness increases with scale, in all basins. Thus, we observe an inversely proportional behaviour of R^2 and F indicating that the more the terrain roughness is attenuated (high F), the more the snow surface roughness can deviate from its underlying terrain forming a distinct winter terrain (low R^2). This confirms quantitatively our intuitive understanding of terrain smoothing. We further observe that terrain smoothing is generally larger (higher F, lower R^2), in basins with

TCD
7, 4633–4680, 2013

low initial roughness. Smoothing is strongest in CB2 where small scale terrain roughness could be almost completely eliminated (F close to 1, R^2 almost 0). With increasing terrain roughness (ST, CB1) terrain smoothing is less pronounced. This behaviour can be best illustrated with the example of 2011 in CB1 and CB2 where the first significant snowfall of the winter season resulted in a very similar snow depth distribution in both basins (Fig. 7). Terrain smoothing is significantly larger (higher F lower R^2) in CB2 than in CB1. This underlines that every basin has a unique imprint and shows a different smoothing behaviour even with almost identical snow depth.

5.2 Terrain smoothing as a function of snow depth

Beside the basin characteristics, it is clear that the differences of the smoothing behaviour observed within every single basin are due to a varying snow cover.

Figure 6 showed qualitatively that terrain smoothing increases with increasing snow depth. In the basin ST for example, we clearly identify two different smoothing behaviours for the two winters of 2010/11 and 2011/12 which were characterized by snow depths in the range 1.33–1.43 m and 1.91–2.75 m, respectively. This pronounced difference in snow depth between the two years results in larger smoothing on scales up to 15 m for the year 2012. On larger scales F of both years converges to values of around 0.4.

However, this behaviour is not unequivocal, and snow depth alone cannot always explain terrain smoothing. For example, the scans of 11 January 2012 and 4 March 2012 show almost the same smoothing behaviour despite a significant larger mean snow depth on 11 January 2012. In this case, the coefficient of variation, C_v, is significantly lower for the scan of 11 January 2012 indicating that the snow cover is less distributed than for 4 March 2012.

This is confirmed in other basins. In CB2 we observe that the smoothing in the year 2006 is only slightly larger than in 2009 despite a significantly thicker snowpack (3.68 m in 2006 compared to 2.13 m in 2009). Also in this case, C_v is almost twice as large in 2009, indicating that relatively more snow has been redistributed. In CB1 we observe

TCD
7, 4633–4680, 2013

that both years 2006 and 2009 show a very similar smoothing behaviour despite higher mean snow depth in 2006. Again, C_v is larger in 2009, thus the snow cover was more affected by redistribution processes.

The above observations suggest that terrain smoothing may thus be dependent on the mean snow depth, $\overline{\mathrm{HS}}$, as well as its variability, $\sigma(\mathrm{HS})$. We define $\widetilde{\mathrm{HS}}$ as $\overline{\mathrm{HS}}$ multiplied by a scaling factor corresponding to the value of its standard deviation, $\sigma(\mathrm{HS})$. Figure 8 shows F with $\widetilde{\mathrm{HS}}$ for the scales of 5 m, 15 m and 25 m and as a comparison only with of $\overline{\mathrm{HS}}$. In both cases, we can see that increasing scales lead to a decreasing smoothing behaviour and that a linear increase in $\overline{\mathrm{HS}}$ and $\widetilde{\mathrm{HS}}$, respectively does not result in a linear increase of the smoothing factor. Therefore, to model terrain smoothing we use a power function, of the form

$$\widetilde{\mathrm{HS}} = c \times F^r, \tag{14}$$

where c and r are coeffcients depending on terrain characteristics and scale. Even if we can observe already a fair correlation (R^2 between 0.27 and 0.67) with $\overline{\mathrm{HS}}$, the quality of the fitting is significantly better when the variability of snow depth is integrated (R^2 between 0.6 and 0.93).

If we solve Eq. (14) for F we obtain:

$$F = \left(\frac{\widetilde{\mathrm{HS}}}{c}\right)^{\frac{1}{r}}, \tag{15}$$

where Table 5 shows charcteristic values of c and r for the basin ST.

The observed smoothing behaviour indicates that the snow which fell at the beginning of the winter season is more efficient in cancelling out roughness than larger snow falls occurring later in the season, when the snow cover is already relatively high. Further, it shows how a simple standard deviation can capture complex redistribution processes such as a wind transport, at least at a basin scale.

However, it is the case that a larger number of scans obtained in all possible snow cover situations would be necessary to confirm and strengthen the significance of this relationship. Nevertheless, we believe that the obtained relation captures well the essence of terrain smoothing. Basins with different terrain characteristics however will probably show a slightly different behaviour with stronger or weaker increase of F in relation to snow depth and its variability. This result shows that, in contrast to the indications given Schweizer et al. (2003), smoothing processes on terrain are not restricted to snow depths of 0.3–1 m, but are still observable in considerably thicker snowpacks. However, it is important to emphasise that this is dependent of the scale of terrain roughness under consideration. Considering the work of Schirmer and Lehning (2011), we can confirm increasing terrain smoothing on increasing scales with a deeper and more variable snowpack, however we did not find a clear break separating scales where terrain is smoothed or not smoothed. We rather observed a gradual decrease of terrain smoothing with increasing scales.

6 Local assessment of snow depth and surface roughness structure

As discussed above, terrain smoothing at the basin scale is directly proportional to the average snow depth and its standard deviation. However, to understand the smoothing behaviour of single terrain features, it is necessary to assess the link between snow depth and surface roughness on a local scale. Accordingly, we analyzed the correlation between snow depth and terrain smoothing on pixel scale (Fig. 9). We can observe that, in contrast to what was observed at basin level, it is not possible to establish a general relationship between the two variables. Thus, to get a deeper understanding of this behaviour we produced gridded maps of 1 m resolution of snow depth and surface roughness and assessed the spatial distribution of snow depth and surface roughness. Figures 10 and 11 show two selected snow depth distributions and the corresponding surface roughness and underlying terrain roughness at a scale of 5 m and 25 m in the basin ST and VdlS, respectively. Maps of all snow depth and roughness distributions can be consulted in the Appendices. Even if a correlation between snow depth and smoothing at the pixel level could not be found, by visual inspection we observe that, snow can influence smoothing processes at feature level, systematically and persistently. This can observed for example in Fig. 10 where channels (marked with black circles) are systematically filled with snow and completely disappear on the surface roughness maps, in all observed scans. Another example is surface roughness due to smaller rocks (marked with yellow circles) which persists in all given snow cover distributions. This illustrates that smoothing processes are strongly driven by single features and explains why a local gridded representation of terrain cannot capture the complex relationship between snow depth and terrain smoothing. The smoothing of a single pixel (in our case 1 m) cannot be unambiguously explained by snow depth and its terrain roughness. It is controlled by geomorphological parameters of neighbouring pixels, which control together with meteorological factors such as wind the local redistribution of snow depending on their arrangement on feature scale. Another reason is that terrain smoothing may vary strongly within an individual basin due to local wind conditions and their interaction with the underlying terrain features which strongly influence deposition, redistribution (e.g. snow drift, saltation, preferential deposition (Lehning et al., 2008; Mott et al., 2010) or wind erosion processes. Surface roughness might thus be influenced by drift features (dunes, cornices) or sastrugi. This complex behaviour is not captured by a simple power law as shown in Sect. 5.2, but can only be reproduced using physical models able to calculate snow redistribution in 3-D terrain (e.g. Alpine 3-D, Lehning et al., 2006).

However we stress that under snow influence, characteristic patterns of surface roughness appear to be persistent. In the following we will thus analyse quantitatively the persistence of snow depth distribution and if this persistence is further transferred to surface roughness.

TCD
7, 4633–4680, 2013

6.1 Inter-annual and intra-annual persistence of snow depth

To quantify intra and inter-annual persistence of snow depth, we calculate the degree of correlation between two distinct winter snow covers using the coefficient of determination, R^2.

Table 4 shows the correlations of the snow depth distribution for the Steintälli basin. We observe high intra-annual correlation of 0.82 between the two scans in the season 2010/11 as well as the five scans in 2011/12 with values ranging from 0.74 to 0.93. Only the scan from 11 January 2012 is correlated to a less strong extent to all other scans from this winter season with values ranging from 0.45 to 0.60. Thus, in general the intra-annual correlation at this site is strong, with higher values towards the middle and end of the accumulation season.

The same holds for the inter-annual comparison. Correlation between scans performed at the beginning of the winter season are generally lower as in the case of scan from 11 January 2012 with the two scans from season 2010/11 ($R^2 = 0.28$ and $R^2 = 0.33$, respectively). The correlation increases for scans performed towards the end of the winter season as in the case of scans from 1 March 2011 and 20 March 2012 ($R^2 = 0.65$).

Table 3 shows correlations of the snow depth distribution for the basins CB1 and CB2. In this case we can only perform an inter-annual comparison, and in agreement with the results from the Steintälli basin, the correlation increases for scans, which correspond to the end of the accumulation season. In fact, we can observe that in basin CB1 the years 2006 and 2009 are more highly correlated ($R^2 = 0.73$) than 2006 and 2009 with 2011 ($R^2 = 0.41$ and $R^2 = 0.34$, respectively). In CB2 this effect is less pronounced, which can be explained by the fact that smooth terrain generally shows lower inter-annual persistence ($R^2 = 0.58$ between 2006 and 2009).

To summarize, we generally observe larger intra-annual and inter-annual persistence for snow depth distributions acquired closer to the end of the accumulation period which have been exposed to settling and redistribution processes over a whole winter. Moreover, we observed weaker intra- and inter-annual consistency for scans performed at the beginning of the season, as the scan from 11 January 2012 in ST or the scan from 8 December 2011 in VdlS. Both scans were acquired in the beginning of the accumulation season and are basically the result of one important single snowfall (or snowfall period in the case of ST). Thus, a single snowfall at the beginning of the accumulation season can considerably vary from the characteristic accumulation pattern. This is in agreement with previous studies of the snow cover distribution which have generally found very high inter-annual persistence of the snow cover at the end of the accumulation season with correlations up to 0.97 (Pearson's correlation coefficient, Schirmer et al., 2011). Yet, inter-annual persistence is slightly lower in the Steintälli basin. This can be explained by large glide snow cracks in the winter season 2011/12, affecting the snow depth distribution during the whole winter season. Still the correlations are significant and the results confirm the hypothesis that the snow cover distribution converges towards a site specific characteristic pattern.

6.2 Inter-annual and intra-annual persistence of surface roughness

In order to quantify the visually observed persistence of roughness, we select in every basin the winter roughness map which we consider the most representative for the field site. This surface serves as a reference for the comparison with all other winter surfaces and the summer terrain roughness. In the basin ST we chose the scan of 20 March 2012, in the two basins CB1 and CB2 the scan of 8 March 2006. We calculated similarity analogously to that in the previous section using the coefficient of determination, R^2.

Tables 6 and 7 show the correlation between the reference surface and all other surfaces (winter and summer) at scales of 5 m, 15 m and 25 m for the basins ST ,CB1 and CB2 respectively. In ST, we observe that the correlation between the reference surface and all other winter surfaces is always larger than the correlation with the summer terrain roughness. Even winter surfaces which were taken in a different winter season compared to the reference surface show this behaviour. Especially on scales where snow has a significant influence meaning that surface roughness is decorrelating from terrain roughness (we consider a threshold of $R^2 < 0.5$), a DTM of a snow surface at peak accumulation explains significantly more of the variance between snow surface roughness and terrain roughness than only the summer terrain. This is even more astonishing as several glide snow cracks in winter 2011/12 introduced considerable alteration in the surface (marked with red circles in Fig. 10).

Further, the same behaviour can be observed in the basins CB1 and CB2. The winter reference surfaces are always more higher correlated to all other winter surfaces than to the terrain surface. Persistence is further increasing with increasing scales, which can partly be explained by the fact that on larger scales, the snow surface is closer linked to terrain. This confirms the observations in our visual assessment that snow surface roughness is highly persistent even in between winter seasons. It is thus potentially possible to capture the persistent characteristics of a winter terrain surface including wind effects without extensive modelling of the snow cover.

7 Conclusions

In this study a method to quantify terrain smoothing based on a multi-scale roughness measure was developed. In addition to previous studies on terrain smoothing, this method allows to quantify the degree of terrain smoothing and link it to geomorphological terrain parameters as the roughness estimates used in our study are based on changes in slope and aspect. Together with the possibility to precisely map roughness changes in the terrain, this is a significant step forward in interpreting terrain smoothing. The analysis on basin scale revealed, that not only mean snow depth but also its variability drive the process of terrain smoothing. In fact, we found that the relation between terrain smoothing and snow depth parameters follows a power law indicating that snowfalls at the beginning of the winter season are more efficient in eliminating roughness than snow falls occurring later in the season. However, more studies would be necessary in the future to confirm this behaviour also in other basins showing dif-

TCD
7, 4633–4680, 2013

ferent terrain characteristics. Furthermore, a relationship between terrain smoothing and snow depth was not found at a pixel level as geomorphology and snow depth of neighbouring pixels strongly influence surface roughness at a given point.

Nevertheless, our results showed that on larger scales winter terrain roughness can be derived, even locally, from a summer DTM using a simple smoothing factor as the relationship between terrain and snow surface roughness is strongly linear. On smaller scales snow surface roughness decorrelates stronger from terrain roughness and the summer DTM is not representative for the winter surface anymore. The critical scale where snow surface decorrelates depends on snow depth and its variability as well as terrain characteristics and has thus to be assessed in each case depending on the current snow situation and the degree of alteration accepted for a given application. Assuming that snow influence is significant for values of $R^2 < 0.5$ between snow surface roughness and terrain roughness, we find critical scales mostly between 5 m and 10 m for snow depth ranging roughly between 1 m and 3 m. Larger critical scales were found in smoother terrain of CB2 with values around 25 m. This finding is very useful to select appropriate resolutions of the DTM for modelling purposes in a winter terrain.

Furthermore, the representation of a winter terrain at resolutions where the influence of snow is high can be significantly improved by the acquisition of a winter DTM close to peak accumulation as it captures site specific and persistent effects of wind-terrain interaction on the snow depth distribution. New technologies to derive high resolution DTMs over a wide area even in a winter terrain have currently been developed (Bühler et al., 2012; Bühler, 2012) and will make it more feasible in the future to obtain those DTMs at significantly lower cost than LIDAR techniques. Such winter terrains may then be very useful in avalanche dynamics simulations (e.g. RAMMS, Christen et al., 2010) as they provide a more realistic estimation of topography. For example the disappearance of small channels observed in a winter terrain can have a large influence on the main direction taken by the flow in 2-D or 3-D simulations. Further the estimation of friction parameters could also be significantly improved. A more realistic winter terrain will thus further improve modelling of wind – ground interaction in snow covered terrain

TCD
7, 4633–4680, 2013

and be important for better snow redistribution simulation, which can be valuable for water resources assessment or ecology purposes.

Moreover, the observed patterns of homogenous snow surface roughness, especially on larger scales (> 10 m), appear to be well suited to defining potential avalanche release areas. We observed that these patterns are generally strongly persistent for different snow depth distributions, however they still diverge locally in some regions. Whereas the persistent parts may represent the zone where an avalanche most often releases, the changes (e.g. connection of two areas with low surface roughness, Fig. 11) may explain the regularly observed differences in release area size and location. This is supported by recent mechanical based – statistical modelling of the slab – weak layer system, which emphasises the important role of small changes in terrain morphology in the definition of release area size (Gaume, 2012). Therefore, automatic procedures for avalanche release area detection (Maggioni and Gruber, 2003; Bühler et al., 2013) and consequently natural hazard management strategies could be improved. However, it is still unclear which scales are critical for the processes determining avalanche release size and location. This has to be assessed in future studies.

Acknowledgements. Funding for this research has been provided through the Interreg project STRADA by the following partners: Amt für Wald Graubünden, Canton du Valais – Service de forêts et paysage, Regione Lombardia, ARPA Lombardia, ARPA Piemonte, Regione Autonoma Valle d'Aosta. The authors would like to thank Walter Steinkogler for helping in the acquisition of the laser scans.

References

Blöschl, G.: Scaling issues in snow hydrology, Hydrol. Process., 13, 2149–2175, 1999. 4636

Bühler, Y.: Remote sensing tools for snow and avalanche research, Proceedings of the 2012 International Snow Science Workshop, Anchorage, Alaska., 264–268, 2012. 4651

Bühler, Y., Marty, M., and Ginzler, C.: High Resolution DEM Generation in High-Alpine Terrain Using Airborne Remote Sensing Techniques, Transactions in GIS, 16, 635–647, 2012. 4651

Bühler, Y., Kumar, S., Veitinger, J., Christen, M., Stoffel, A., and Snehmani: Automated identification of potential snow avalanche release areas based on digital elevation models, Natural Hazards and Earth System Science, 13, 1321–1335, 2013. 4635, 4652

Christen, M., Kowalski, J., and Bartelt, P.: RAMMS: Numerical simulation of dense snow avalanches in three-dimensional terrain, Cold Reg. Sci. Technol., 63, 1–14, 2010. 4651

Deems, J. S., Fassnacht, S. R., and Elder, K. J.: Fractal Distribution of Snow Depth from Lidar Data, J. Hydrometeorol., 7, 285–297, 2006. 4636

Deems, J. S., Fassnacht, S. R., and Elder, K. J.: Interannual Consistency in Fractal Snow Depth Patterns at Two Colorado Mountain Sites, J. Hydrometeor., 9, 977–988, 2008. 4636

Fassnacht, S., Williams, M., and Corrao, M.: Changes in the surface roughness of snow from millimetre to metre scales, Ecological Complexity, 6, 221–229, 2009. 4635

Fischer, L., Eisenbeiss, H., Kääb, A., Huggel, C., and Haeberli, W.: Monitoring topographic changes in a periglacial high-mountain face using high-resolution DTMs, Monte Rosa East Face, Italian Alps, Permafrost and Periglacial Processes, 22, 140–152, 2011. 4636

Gaume, J.: Evaluation of avalanche release depths. Combined statistical mechanical modeling, Ph.D. thesis, Université de Grenoble, 2012. 4652

Grohmann, C., Smith, M., and Riccomini, C.: Multiscale Analysis of Topographic Surface Roughness in the Midland Valley, Scotland, IEEE T. Geosci. Remote, 49, 1200–1213, 2011. 4637

Grünewald, T., Schirmer, M., Mott, R., and Lehning, M.: Spatial and temporal variability of snow depth and ablation rates in a small mountain catchment, The Cryosphere, 4, 215–225, doi:10.5194/tc-4-215-2010, 2010. 4636

Hobson, R. D.: Surface roughness in topography: a quantitative approach, pp. 221–245, Harper & Row, 1972. 4638

Horn, B. K. P.: Hill shading and the reflectance map, Proceedings of the IEEE, 69, 14–47, 1981. 4638

Lehning, M., Völksch, I., Gustafsson, D., Nguyen, T. A., Stähli, M., and Zappa, M.: ALPINE3D: a detailed model of mountain surface processes and its application to snow hydrology, Hydrol. Process., 20, 2111–2128, 2006. 4647

Lehning, M., Löwe, H., Ryser, M., and Raderschall, N.: Inhomogeneous precipitation distribution and snow transport in steep terrain, Water Resour. Res., 44, W07404, doi:10.1029/2007WR006545, 2008. 4647

TCD
7, 4633–4680, 2013

Influence of snow depth distribution on surface roughness in alpine terrain

J. Veitinger et al.

Lehning, M., Grünewald, T., and Schirmer, M.: Mountain snow distribution governed by an altitudinal gradient and terrain roughness, Geophys. Res. Lett., 38, L19504, doi:10.1029/2011GL048927, 2011. 4637

Maggioni, M. and Gruber, U.: The influence of topographic parameters on avalanche release dimension and frequency, Cold Reg. Sci. Technol., 37, 407–419, 2003. 4635, 4652

Manninen, T., Anttila, K., Karjalainen, T., and Lahtinen, P.: Automatic snow surface roughness estimation using digital photos, J. Glaciol., 58, 993–1007, 2012. 4635

McClung, D.: Characteristics of terrain, snow supply and forest cover for avalanche initiation caused by logging, Ann. Glaciol., 32, 223–229, 2001. 4635

McClung, D. M. and Schaerer, P. A.: The Avalanche Handbook, Seattle, WA, the mountaineers edn., 2002. 4636

Mott, R., Schirmer, M., Bavay, M., Grünewald, T., and Lehning, M.: Understanding snow-transport processes shaping the mountain snow-cover, The Cryosphere, 4, 545–559, doi:10.5194/tc-4-545-2010, 2010. 4635, 4647

Prokop, A.: Assessing the applicability of terrestrial laser scanning for spatial snow depth measurements, Cold Reg. Sci. Technol., 54, 155–163, 2008. 4636

Prokop, A., Schirmer, M., Rub, M., Lehning, M., and Stocker, M.: A comparison of measurement methods: terrestrial laser scanning, tachymetry and snow probing for the determination of the spatial snow-depth distribution on slopes, Ann. Glaciol., 49, 210–216, 2008. 4636

Sappington, J., Longshore, K., and Thomson, D.: Quantifiying Landscape Ruggedness for Animal Habitat Anaysis: A case Study Using Bighorn Sheep in the Mojave Desert, J. Wildl. Manage., 71, 1419–1426, 2007. 4637, 4639, 4664

Schirmer, M. and Lehning, M.: Persistence in intra-annual snow depth distribution: 2.Fractal analysis of snow depth development, Water Resour. Res., 47, W09517, doi:10.1029/2010WR009429, 2011. 4636, 4637, 4646

Schirmer, M., Wirz, V., Clifton, A., and Lehning, M.: Persistence in intra-annual snow depth distribution: 1.Measurements and topographic control, Water Resour. Res., 47, W09516, doi:10.1029/2010WR009426, 2011. 4636, 4649

Schweizer, J., Bruce Jamieson, J., and Schneebeli, M.: Snow avalanche formation, Rev. Geophys., 41, 1016, doi:10.1029/2002RG000123, 2003. 4635, 4637, 4646

Simenhois, R. and Birkeland, K. W.: The effect of changing slab thickness on fracture propagation, Proceedings of the 2008 International Snow Science Workshop, Whistler, B.C., 755–760, 2008. 4635

TCD
7, 4633–4680, 2013

Sovilla, B., McElwaine, J. N., Schaer, M., and Vallet, J.: Variation of deposition depth with slope angle in snow avalanches: Measurements from Vallée de la Sionne, J. Geophys. Res., 115, F02016, doi:10.1029/2009JF001390, 2010. 4642

Sovilla, B., Sonatore, I., Bühler, Y., and Margreth, S.: Wet-snow avalanche interaction with a deflecting dam: field observations and numerical simulations in a case study, Nat. Hazards Earth Syst. Sci., 12, 1407–1423, doi:10.5194/nhess-12-1407-2012, 2012. 4639

Trujillo, E., Ramirez, J. A., and Elder, K. J.: Topographic, meteorologic, and canopy controls on the scaling characteristics of the spatial distribution of snow depth fields, Water Resour. Res., 43, W07409, doi:10.1029/2006WR005317, 2007. 4636

Vallet, J.: Quick Deployment Heliborne Handheld LiDAR System for Natural Hazard Mapping, 3–7 May, in: Gi4DM – Geoinformation for Disaster management Conference, Antalya, Turkey, 2011. 4636

van Herwijnen, A. and Heierli, J.: Measurement of crack-face friction in collapsed weak snow layers, Geophys. Res. Lett., 36, L23502, doi:10.1029/2009GL040389, 2009. 4636

Vontobel, I.: Geländeanalysen von Unfalllawinen, Master's thesis, Department of Geography, University of Zurich, 2011. 4639

Winstral, A., Elder, K., and Davis, R. E.: Spatial Snow Modeling of Wind-Redistributed Snow Using Terrain-Based Parameters, J. Hydrometeor, 3, 524–538, 2002. 4636

TCD
7, 4633–4680, 2013

Table 1. Mean $\overline{\mathrm{HS}}$, standard deviation $\sigma(\mathrm{HS})$ and coefficient of variation C_v of snow depth distribution for every laser scan aquistion in the ST basin.

Steintälli			
Date	$\overline{\mathrm{HS}}$	$\sigma(\mathrm{HS})$	C_v
(1) 2 Feb 2011	1.33	0.48	0.36
(2) 1 Mar 2011	1.43	0.53	0.37
(3) 11 Jan 2012	2.75	0.54	0.20
(4) 13 Feb 2012	1.91	0.60	0.32
(5) 4 Mar 2012	1.99	0.73	0.36
(6) 9 Mar 2012	2.31	0.70	0.30
(7) 20 Mar 2012	2.01	0.75	0.37

TCD
7, 4633–4680, 2013

TCD
7, 4633–4680, 2013

Influence of snow depth distribution on surface roughness in alpine terrain

J. Veitinger et al.

Table 2. Mean $\overline{\mathrm{HS}}$, standard deviation σ(HS) and coefficient of variation C_v of snow depth distribution for every laser scan aquistion in the CB1 and CB2 basins.

Date	$\overline{\mathrm{HS}}$	σ(HS)	C_v
Crêta Besse 1			
(1) 8 Mar 2006	2.71	0.78	0.29
(2) 25 Jan 2009	1.36	0.64	0.47
(3) 8 Dec 2011	1.39	0.30	0.22
Crêta Besse 2			
(1) 8 Mar 2006	3.68	0.61	0.17
(2) 25 Jan 2009	2.13	0.62	0.29
(3) 8 Dec 2011	1.36	0.23	0.17

Table 3. Correlation R^2 of snow depth values in the CB1 and CB2 basins.

	2006	2009	2011
Crêta Besse 1			
2006	1		
2009	0.73	1	
2011	0.41	0.34	1
Crêta Besse 2			
2006	1		
2009	0.58	1	
2011	0.54	0.29	1

TCD
7, 4633–4680, 2013

Table 4. Correlation R^2 of snow depth values in the ST basin.

Steintälli							
Date	(1)	(2)	(3)	(4)	(5)	(6)	(7)
(1) 2 Feb 2011	1						
(2) 1 Mar 2011	0.82	1					
(3) 11 Jan 2012	0.28	0.33	1				
(4) 13 Feb 2012	0.39	0.54	0.60	1			
(5) 4 Mar 2012	0.55	0.66	0.46	0.82			
(6) 9 Mar 2012	0.57	0.59	0.56	0.80	0.87	1	
(7) 20 Mar 2012	0.63	0.65	0.45	0.74	0.91	0.93	1

TCD
7, 4633–4680, 2013

Influence of snow depth distribution on surface roughness in alpine terrain

J. Veitinger et al.

Table 5. Coefficients c and r of the power function modelling terrain smoothing in the basin of ST.

Steintälli		
Scale	c	r
5 m	2.8	2.1
15 m	11.6	3.3
25 m	22.7	3.3

TCD
7, 4633–4680, 2013

Table 6. Correlation R^2 of surface roughness of winter scan (7) from 20 March 2012 with other winter scans and summer terrain in the ST basin.

Steintälli							
Scale	(1)	(2)	(3)	(4)	(5)	(6)	DTM
5 m	0.45	0.47	0.41	0.52	0.79	0.77	0.30
15 m	0.67	0.67	0.72	0.77	0.94	0.97	0.62
25 m	0.79	0.79	0.86	0.88	0.97	0.97	0.76

TCD
7, 4633–4680, 2013

Table 7. Correlation R^2 of surface roughness of winter scan (1) from 8 March 2006 with other winter scans and summer terrain in the CB1 and CB2 basins.

Crêta Besse 1			
Scale	2009	2011	DTM
5 m	0.63	0.49	0.39
15 m	0.89	0.84	0.78
25 m	0.95	0.92	0.88
Crêta Besse 2			
Scale	2006	2011	DTM
5 m	0.38	0.31	0.10
15 m	0.75	0.67	0.36
25 m	0.83	0.81	0.53

TCD
7, 4633–4680, 2013

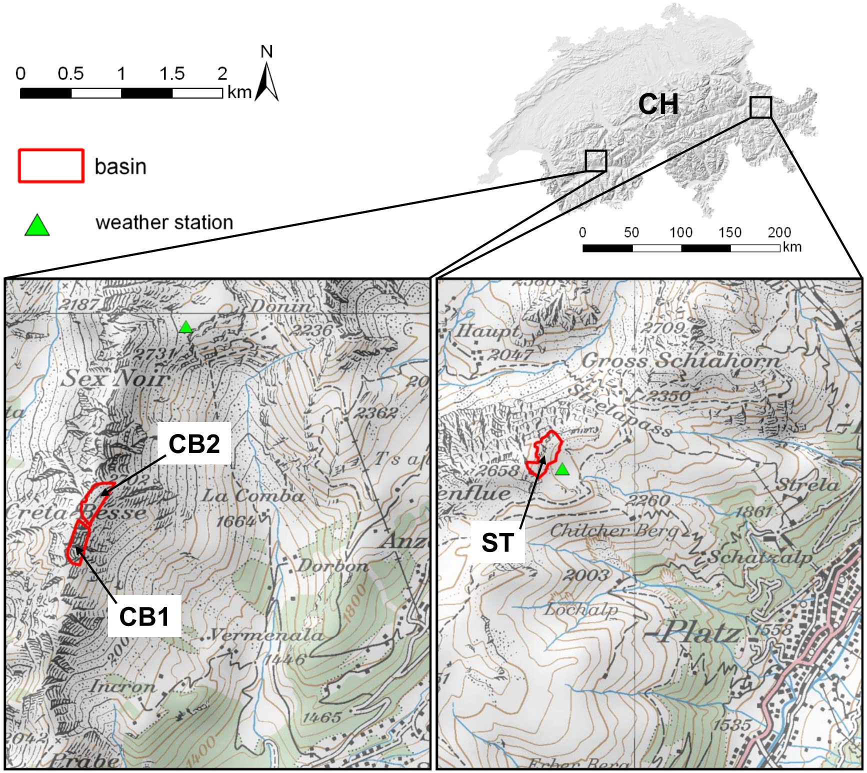

Fig. 1. Location of the fieldsites Vallée de la Sionne (left) and Steintälli (right). In red are marked the the exact location of the analyzed basins CB1, CB2 and ST and in green the location of the weather stations.

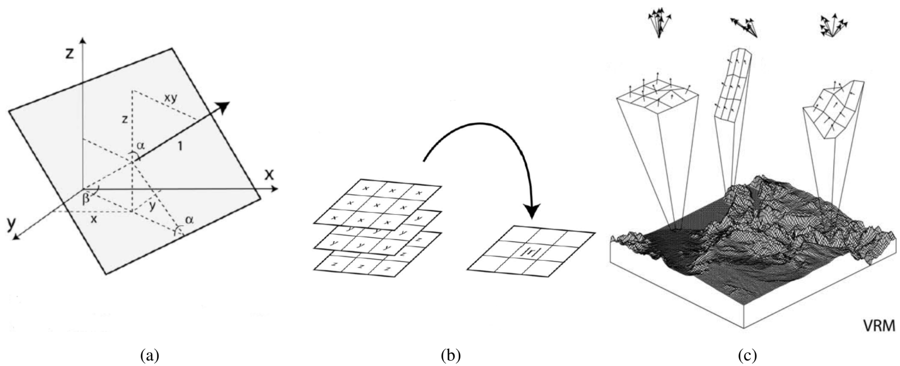

Fig. 2. Calculation of vector ruggedness measure VRM. **(a)** Decomposition of normal unit vectors of a DTM grid cell into x, y, z components using slope α and aspect β. **(b)** Resultant vector r is obtained by summing up all x, y, z components of the whole neighborhood window. **(c)** Vector ruggedness measure in flat (left), steep and even (middle) as well as steep and uneven terrain (right). Graphics from Sappington et al. (2007).

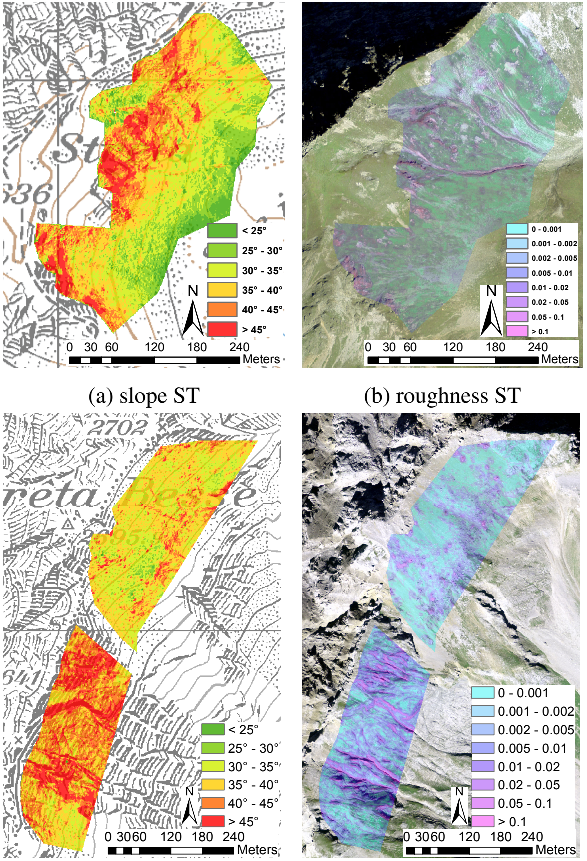

(a) slope ST

(b) roughness ST

(c) slope VdlS

(d) roughness VdlS

Fig. 3. Geomorphological characterization of the Steintälli and the Vallée de la Sionne basins. **(a)**, **(c)** Slope derived from a DTM with 1 m resolution and **(b)**, **(d)** roughness derived from a DTM with 1 m resolution, for a 5 m scale.

TCD
7, 4633–4680, 2013

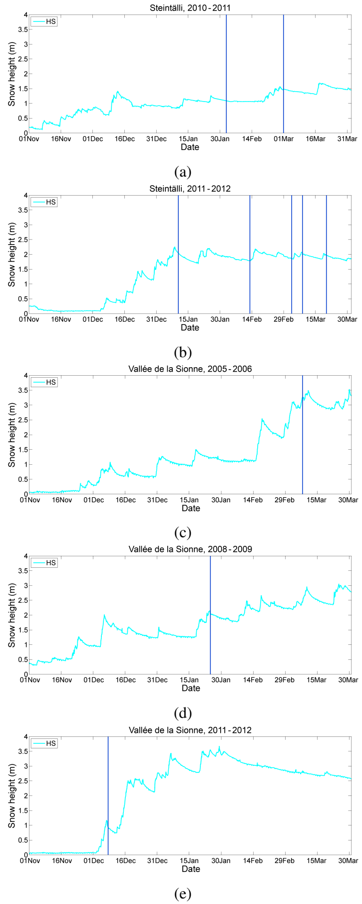

Fig. 4. Evolution of snow depth from 1 November until 31 March at **(a)** and **(b)** the weather station WAN7 in Steintälli and **(c–e)** at the weather station Donin du Jour in the Vallée de la Sionne. The vertical blue lines correspond to the acquisition times of the laser scans.

TCD
7, 4633–4680, 2013

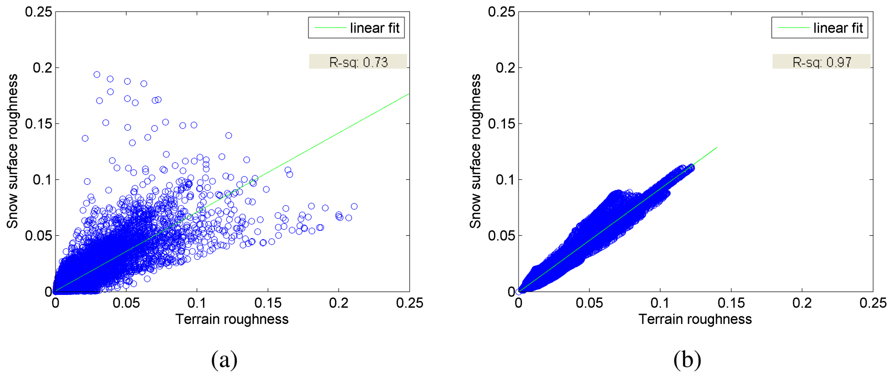

Fig. 5. Snow surface roughness as a function of terrain roughness in CB1 in the year 2011 for scales of **(a)** 5 m and **(b)** 25 m.

TCD
7, 4633–4680, 2013

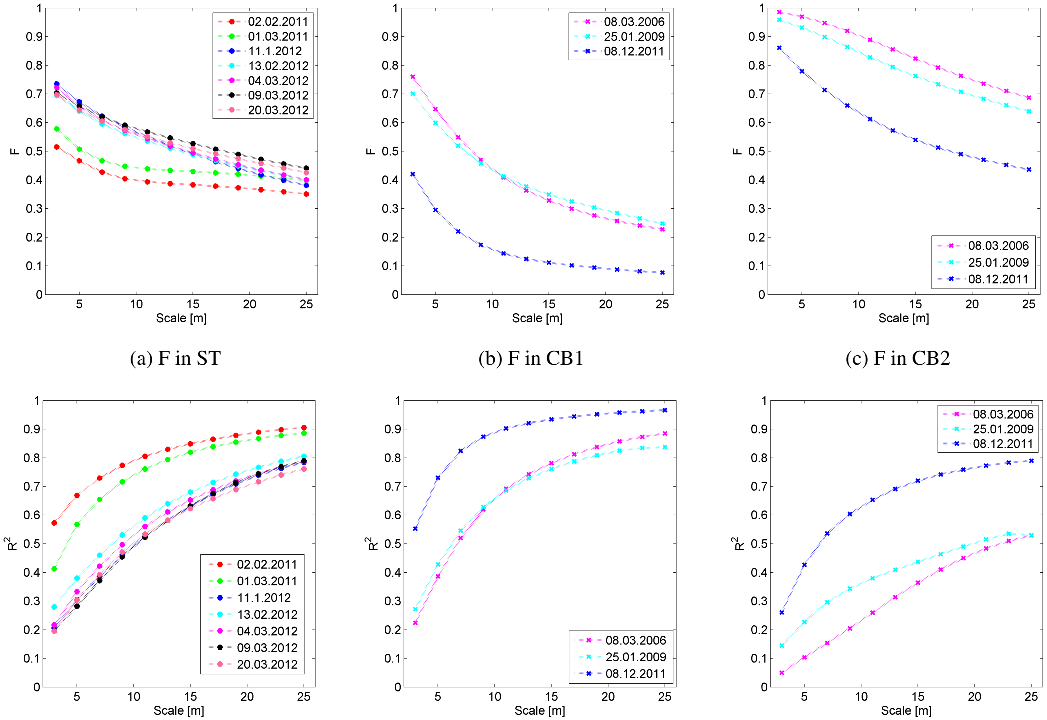

(a) F in ST (b) F in CB1 (c) F in CB2

(d) R^2 in ST (e) R^2 in CB1 (f) R^2 in CB2

Fig. 6. (a–c) Smoothing factor F and **(d–f)** coefficient of determination R^2 between snow suraface roughness and terrain roughness as a function of scale for the basins ST, CB1 and CB2.

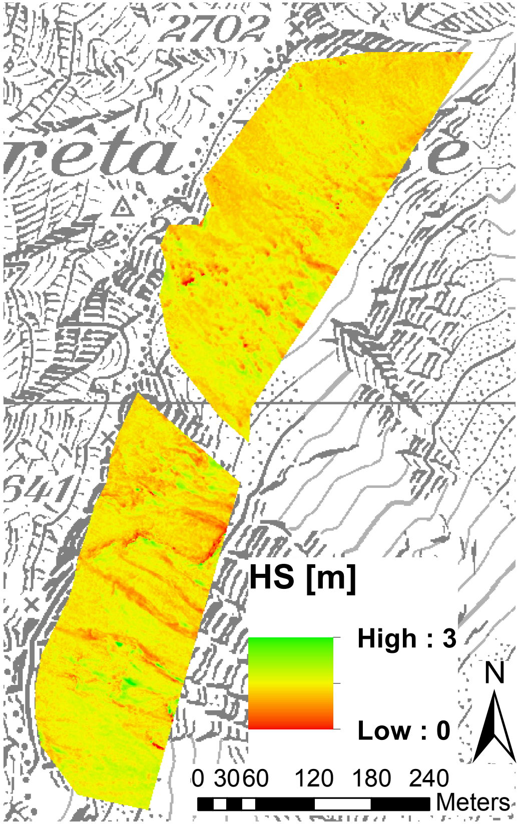

Fig. 7. Snow depth in the basins CB1 and CB2 on 8 December 2011.

TCD
7, 4633–4680, 2013

Influence of snow depth distribution on surface roughness in alpine terrain

J. Veitinger et al.

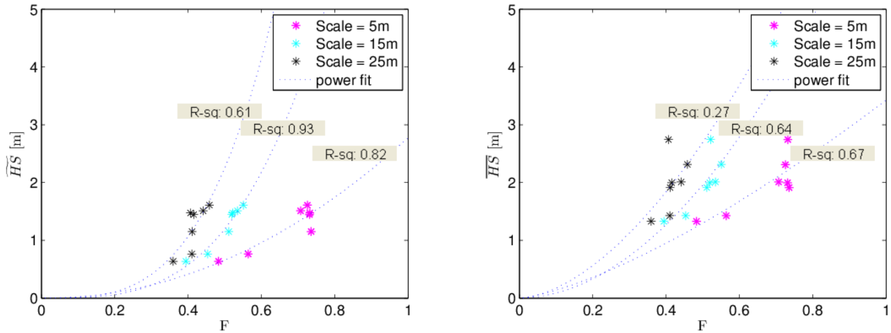

(a) (b)

Fig. 8. (a) *F* with mean snow depth multiplied by a scaling factor corresponding to its standard deviation and **(b)** *F* only with mean snow depth for scales 5 m, 15 m and 25 m.

TCD
7, 4633–4680, 2013

TCD
7, 4633–4680, 2013

Influence of snow depth distribution on surface roughness in alpine terrain

J. Veitinger et al.

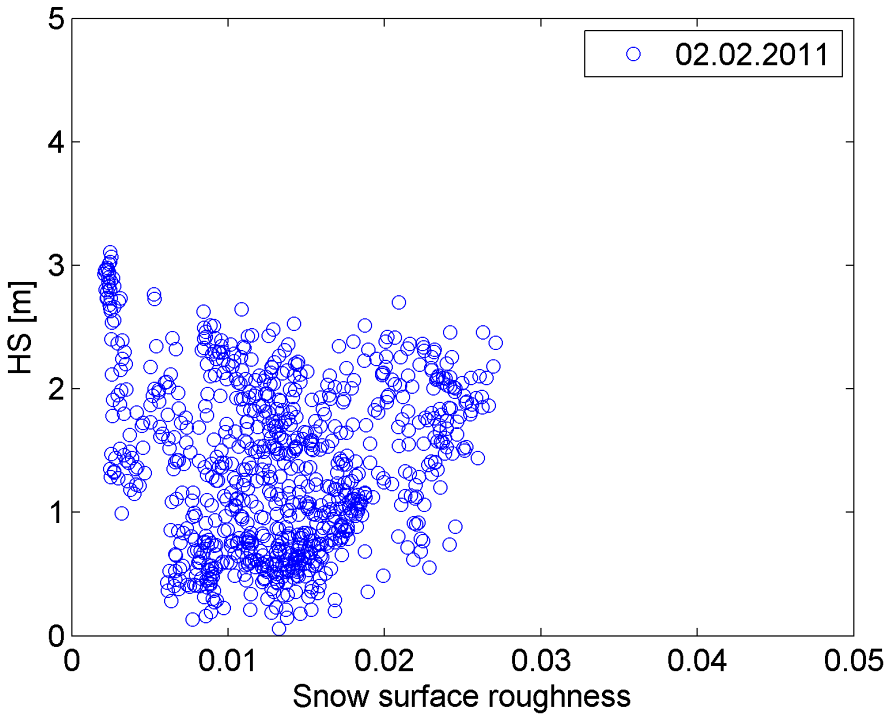

Fig. 9. Snow surface roughness as a function of snow depth for terrain roughness of 0.025 ± 0.001. Example for aquistion of 2 February 2011 and a scale of 15 m in the basin ST.

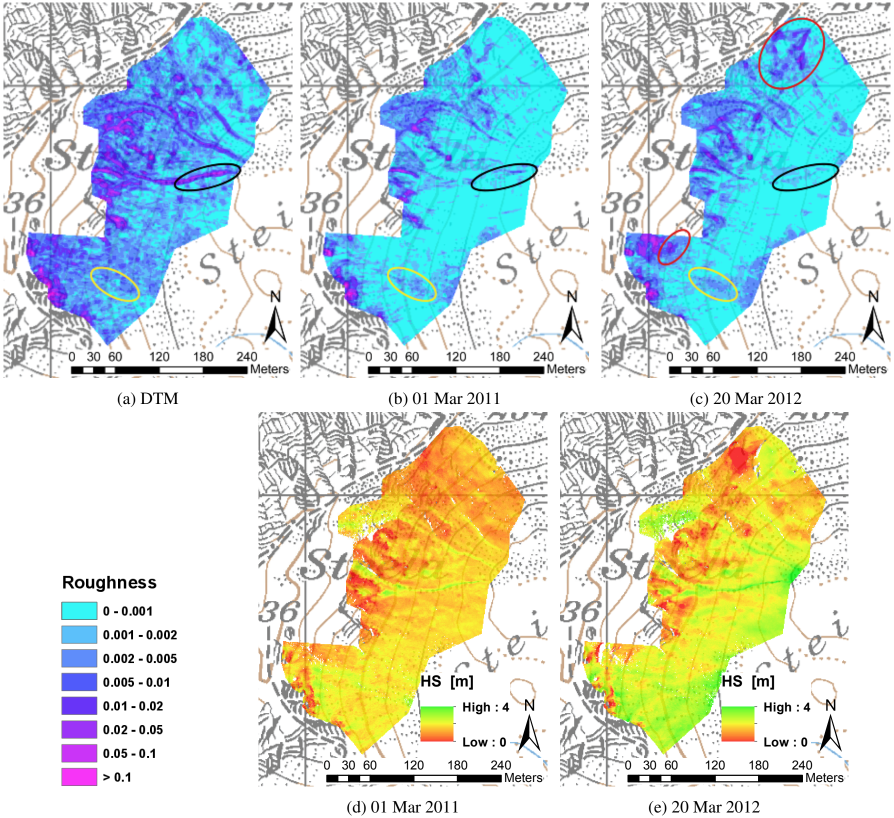

Fig. 10. **(a)** Surface roughness of summer terrain and **(b)**, **(c)** winter terrain at a scale of 5m in the basin ST. **(d)**, **(e)** show the corresponding snow depth distributions. The black and yellow circles show persistent smoothing features. Red circles show the location of glide snow cracks.

TCD
7, 4633–4680, 2013

TCD
7, 4633–4680, 2013

Influence of snow depth distribution on surface roughness in alpine terrain

J. Veitinger et al.

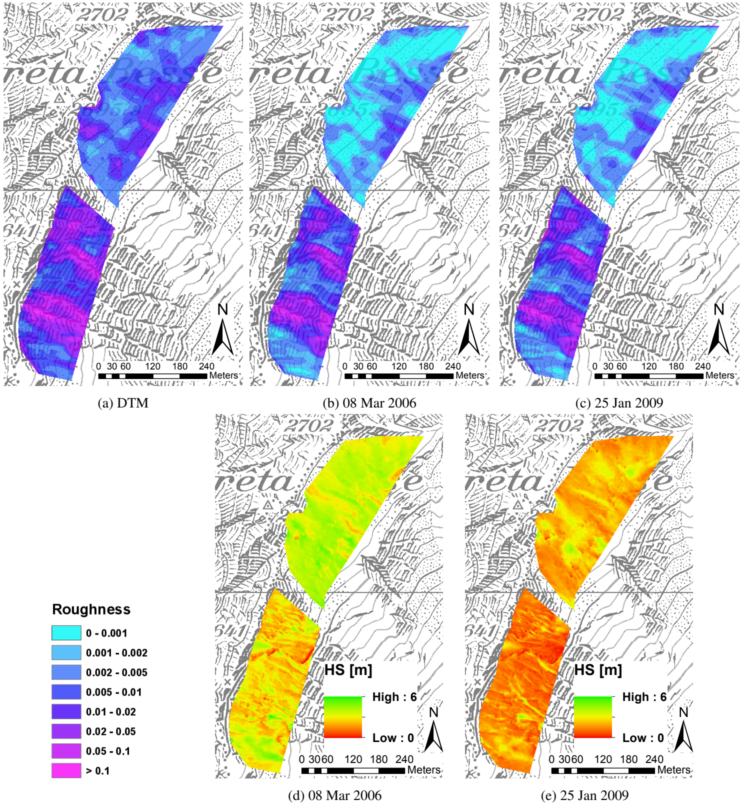

Fig. 11. **(a)** Surface roughness of summer terrain and **(b)**, **(c)** winter terrain at a scale of 25 m in the basins CB1 and CB2. **(d)**, **(e)** show the corresponding snow depth distributions.

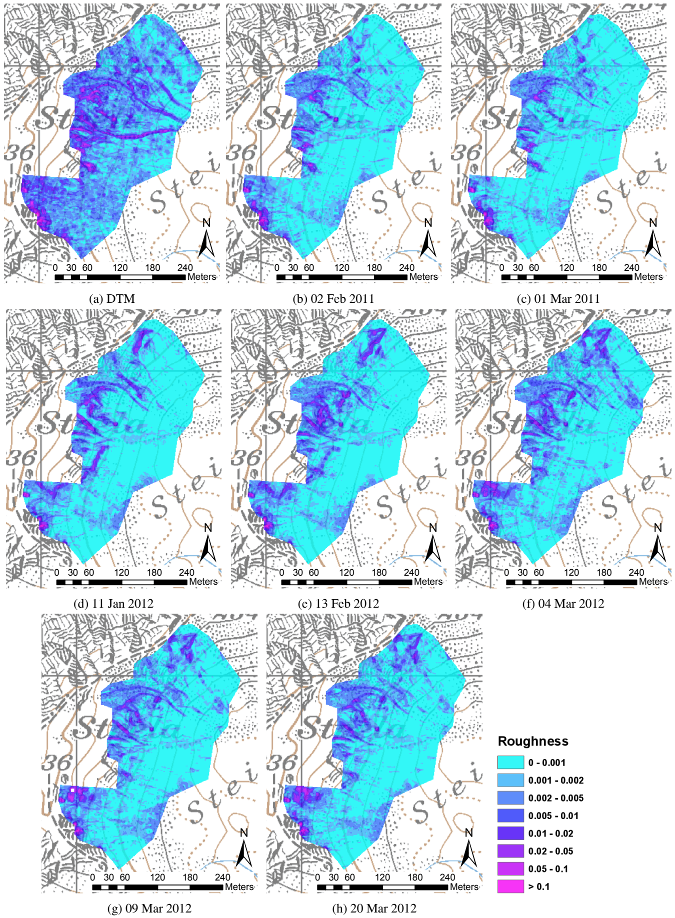

Fig. A1. Surface roughness of summer terrain and winter terrain at a scale of 5 m in the basin ST.

TCD
7, 4633–4680, 2013

Influence of snow depth distribution on surface roughness in alpine terrain

J. Veitinger et al.

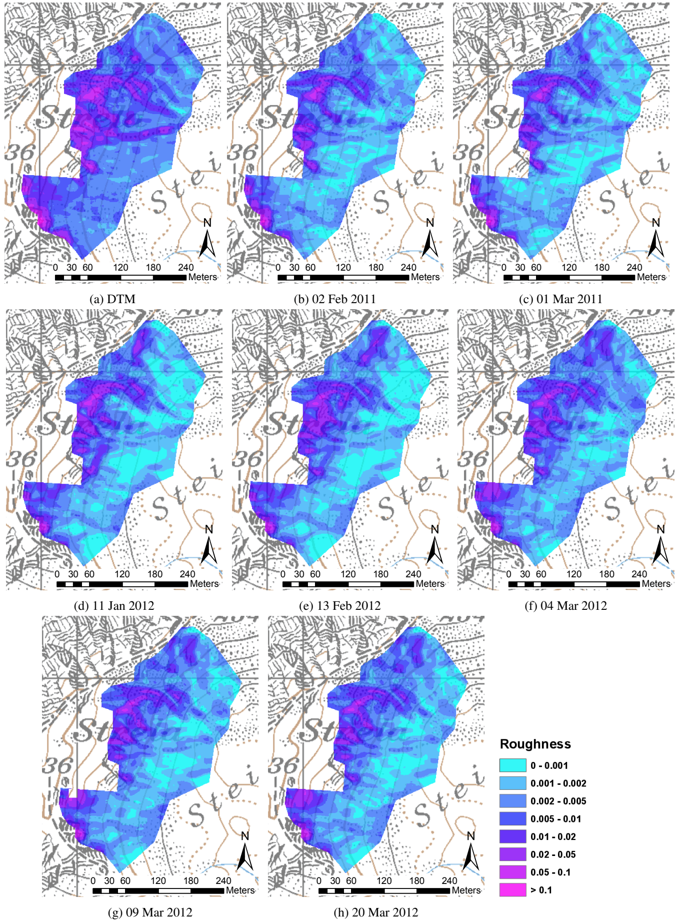

Fig. A2. Surface roughness of summer terrain and winter terrain at a scale of 15 m in the basin ST.

TCD
7, 4633–4680, 2013

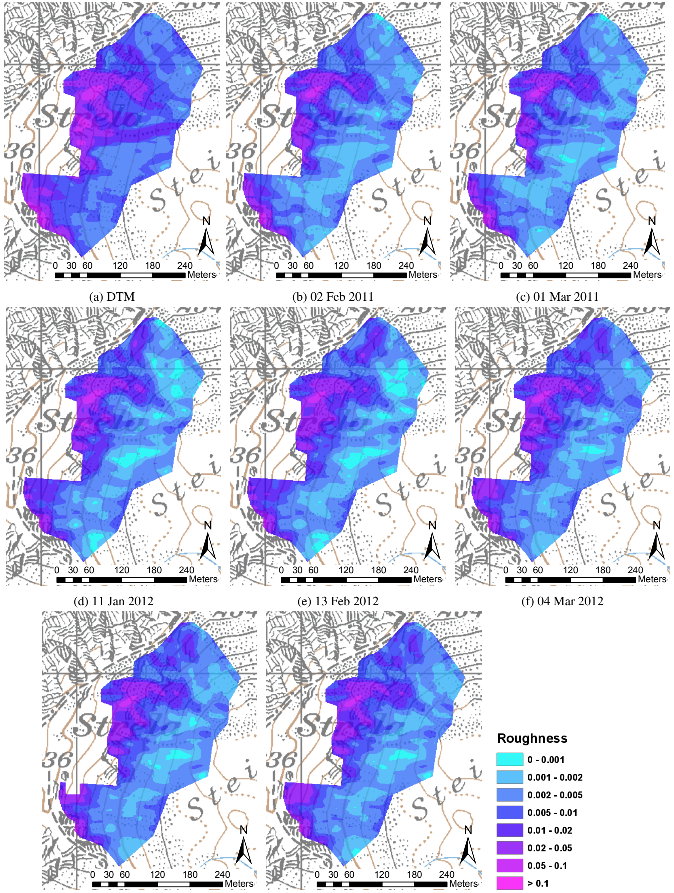

(a) DTM (b) 02 Feb 2011 (c) 01 Mar 2011
(d) 11 Jan 2012 (e) 13 Feb 2012 (f) 04 Mar 2012
(g) 09 Mar 2012 (h) 20 Mar 2012

Fig. A3. Surface roughness of summer terrain and winter terrain at a scale of 25 m in the basin ST.

TCD
7, 4633–4680, 2013

Title Page
Abstract Introduction
Conclusions References
Tables Figures
◂◂ ▸▸
◂ ▸
Back Close
Full Screen / Esc
Printer-friendly Version
Interactive Discussion

Discussion Paper | Discussion Paper | Discussion Paper | Discussion Paper |

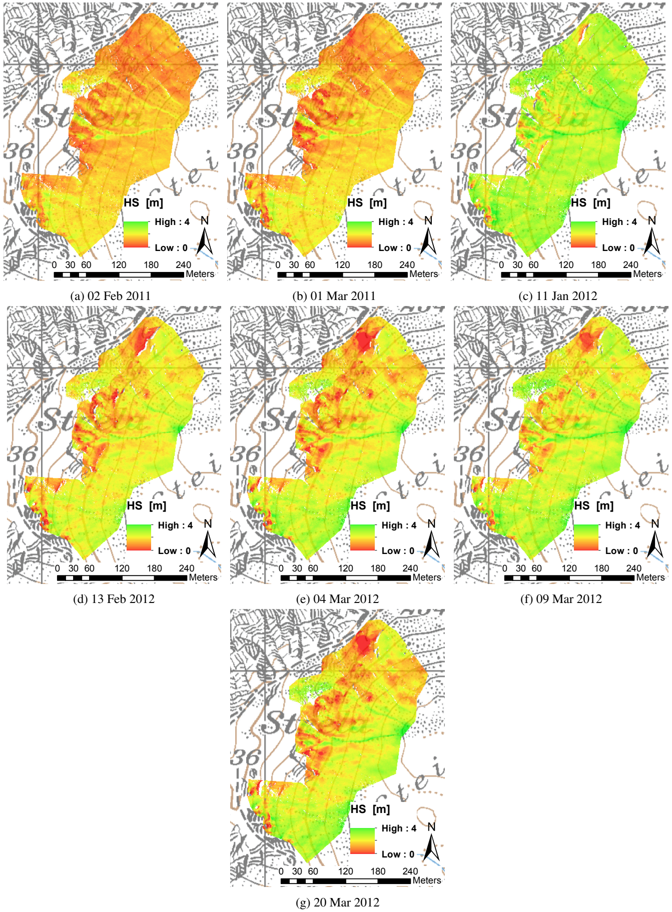

Fig. A4. Snow depth distributions in the basin ST.

TCD
7, 4633–4680, 2013

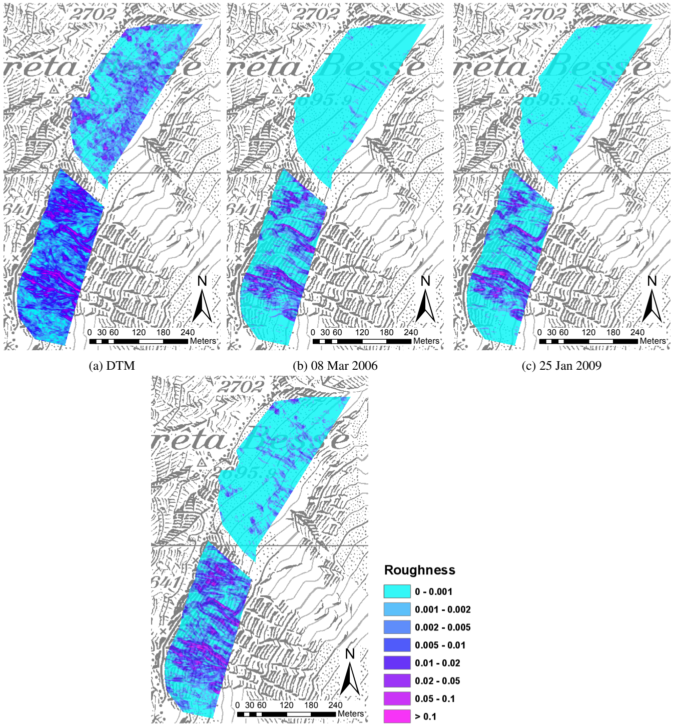

Fig. A5. Surface roughness of summer terrain and winter terrain at a scale of 5 m in basins CB1 and CB2.

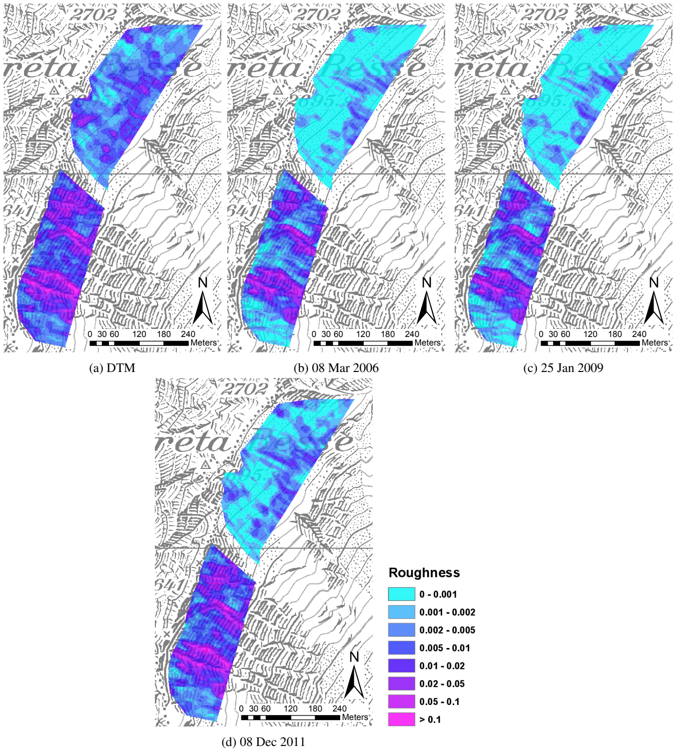

Fig. A6. Surface roughness of summer terrain and winter terrain at a scale of 15 m in basins CB1 and CB2.

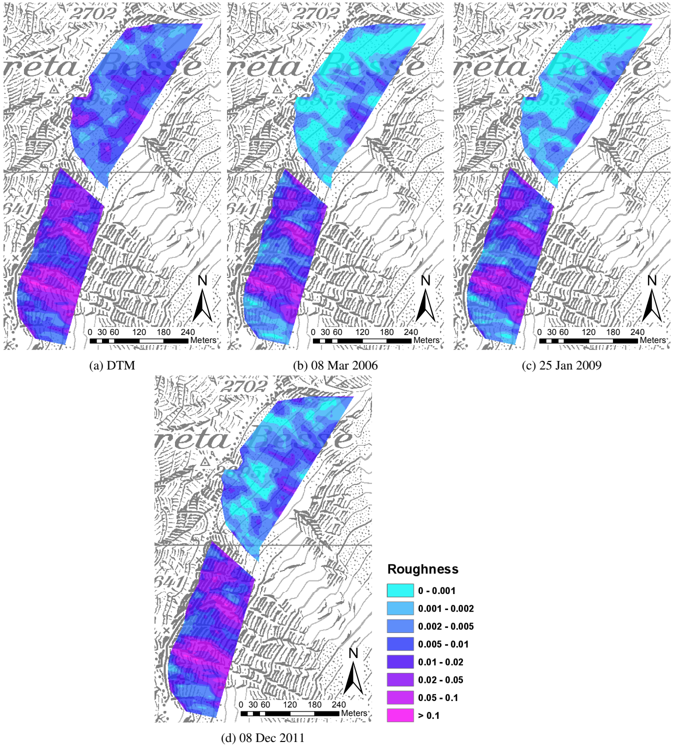

Fig. A7. Surface roughness of summer terrain and winter terrain at a scale of 25 m in basins CB1 and CB2.

TCD

7, 4633–4680, 2013

Influence of snow depth distribution on surface roughness in alpine terrain

J. Veitinger et al.